Size-resolved exposure risk of persistent free radicals (PFRs) in atmospheric aerosols and their potential sources

Qingcai Chen,[a,] Haoyao Sun,[a,] Wenhuai Song,[b] Fang Cao,[b] Chongguo Tian,[c] Yan-Lin Zhang[b*]

[a] *School of Environmental Science and Engineering, Shaanxi University of Science and Technology, Xi'an 710021, China*

[b] *Yale–NUIST Center on Atmospheric Environment, International Joint Laboratory on Climate and Environment Change (ILCEC), Nanjing University of Information Science and Technology, Nanjing 210044, China*

[c] *Key Laboratory of Coastal Environmental Processes and Ecological Remediation, Yantai Institute of Coastal Zone Research, Chinese Academy of Sciences, Yantai, 264003, China*

[*]Corresponding Author at: Ningliu Road 219, Nanjing 210044, China.

E-mail address: dryanlinzhang@outlook.com or zhangyanlin@nuist.edu.cn (Yan-Lin Zhang).

Abstract: Environmentally persistent free radicals (EPFRs) are a new type of substance with potential health risks. EPFRs are widely present in atmospheric particulates, but there is a limited understanding of the size-resolved health risks of these radicals. This study reports the exposure risks and source of EPFRs in atmospheric particulate matter (PM) of different particle sizes (<10 μm) in Linfen, a typical coal-burning city in China. The type of EPFRs in fine particles (< 2.1 μm) is different from that in coarse particles (2.1-10 μm) in both winter and summer. However, the EPFR concentration is higher in coarse particles than in fine particles in summer, and the opposite trend is found in winter. In both seasons, combustion sources are the main sources of EPFRs with coal combustion as the major contributor in winter, while other fuel combustions are the major source in summer. Dust contributes part of the EPFRs and it is mainly present in coarse particles in winter and the opposite in summer. The upper respiratory tract was found to be the area with the highest risk of exposure to EPFRs of the studied aerosols, with an exposure equivalent to that of approximately 21 cigarettes per person per day. Alveolar exposure to EPFRs is equivalent to 8 cigarettes per person per day, with combustion sources contributing the most to EPFRs in the alveoli. This study helps us to better understand the potential health risks of atmospheric PM with different particle sizes.

Key words: EPFRs; particle size distribution; source; generation process

34 **TOC Art:**

35
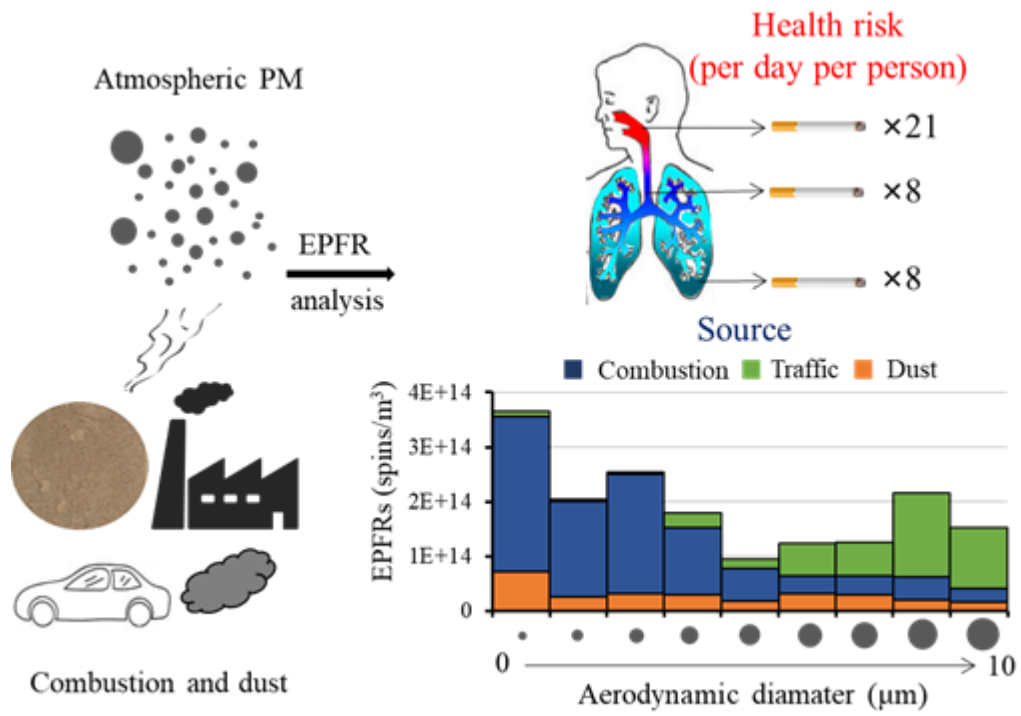
1. Introduction

Free radicals are atoms or groups containing unpaired electrons, such as hydroxyl radicals and superoxide radicals, and they usually have strong chemical reactivity and short lifetimes (Pryor et al., 1986; Finkelstein., 1982). Free radicals with long lifetimes (months or even years) in the environment are currently called environmentally persistent free radicals (EPFRs), which have received much attention in recent years as new environmentally hazardous substances (Vejerano et al., 2018; Gehling, 2013; Chen et al., 2019c). EPFRs can be used as an active intermediate to catalyze the production of reactive oxygen species (ROS) by oxygen molecules, thus endangering human health (D'Arienzo et al., 2017; Thevenot et al., 2013; Harmon et al., 2018; Blakley et al., 2001; Khachatryan et al., 2011). Studies have found that EPFRs are present in different environmental media, such as water and soil, and even in the atmosphere (Dellinger et al., 2001; Truong et al., 2010; Vejerano et al., 2012).

A number of studies have investigated the occurrences, sources and formation process of EPFRs in atmospheric particulates in different regions. For example, in the studies of Rostock in Germany, Taif in Saudi Arabia and Xuanwei in China, the average concentration of EPFRs in atmospheric particulate matter (PM) was reported to be in the range of ~ 10^{16} - 10^{18} spins/g (Wang et al., 2018; Arangio et al., 2016; Shaltout et al., 2015). Atmospheric EPFRs are mainly carbon-centered radicals with adjacent oxygen atoms (Gehling et al., 2013). EPFRs of different lifetimes are present in atmospheric PM, with only a few hours for short-lifetime EPFRs and several years for long-lifetime EPFRs that show no signs of decay (Gehling et al., 2013; Chen et al., 2019c). Most studies indicate that sources of transportation and combustion may be the primary EPFR sources in atmospheric PM (Wang et al., 2018; Yang et al., 2017; Chen et al., 2019b). Chen et al. (2018b and 2019b) found that strong atmospheric photochemical effects in summer and dust particles may also be important sources of EPFRs. The process of electron transfer and stabilization between the surface of metal oxides (such as iron, copper, zinc and nickel) and substituted aromatic molecules

64　under high temperatures is considered to be the main process for the formation of

65　EPFRs in atmospheric particles (Truong., 2010; Vejerano et al., 2012a; Patterson et al.,

66　2013; Vejerano., 2010; Vejerano et al., 2012b). However, the study by Chen et al.

67　(2018a) suggests that EPFRs in atmospheric particulates are mainly derived from

68　graphite oxide-like substances produced during combustion. In addition to primary

69　sources such as combustion, secondary chemical processes in the atmosphere may

70　also be an important source of EPFRs in atmospheric PM (Chen et al. 2019b and

71　2019d; Tong et al., 2018).

72　Different particle sizes of atmospheric PM pose different health risks to humans,

73　depending on the deposition efficiency of the particles and the chemical composition

74　and concentrations of hazardous substances they contain (Strak et al., 2012;

75　Valavanidis et al., 2008). Among various hazardous substances, EPFRs may also be

76　involved in the toxicity of atmospheric particulates. Yang et al. (2017) studied the the

77　EPFRs that are extractable by dichloromethane in different particle sizes in Beijing in

78　winter and found that the concentration of EPFRs was the highest in particles with

79　sizes < 1 μm. Arangio et al. (2016) found that the concentration of EPFRs in 180 nm

80　particles was the highest in the 56 nm - 1.8 μm particle size range. Although several

81　studies have examined the particle size distribution of EPFRs, systematic studies have

82　not been conducted on the formation process, source and exposure assessment of

83　EPFRs in atmospheric particles with different particle sizes.

84　This study takes Linfen as an example. Linfen is one of the cities in China with

85　the most serious air pollution and is a typical coal-burning city. The particle size

86　distribution of EPFRs in atmospheric PM in this region was studied by EPR

87　spectrometry. The effects of particle size and season on the source, formation process,

88　and health risk of EPFRs were revealed. In particular, the comprehensive health risks

89　of EPFRs were evaluated, and it was found that the upper respiratory tract is the area

90　with the highest risk of EPFRs exposure, which is equivalent to twenty-one cigarettes

91　per person per day. This study is of great significance for understanding the source

92　and formation process of EPFRs in atmospheric particulates as well as for health risk

93 assessments.

2. Experimental section

2.1 Sample collection

96   The sampling site for this study is located in Hongdong (36°23', 111°40'E) in
97 Shanxi, China. To collect atmospheric particles of different sizes (0-10 μm), this study
98 used a Thermo-Anderson Mark II sampler to collect aerosol samples of 9 sizes. The
99 samples were collected on a prebaked quartz filter (450 °C, 4.5 hours), and the
100 sampling dates were as follows: in winter, January 26 to February 4, 2017, $n = 10$; and
101 in summer, July 31 to August 24, 2017, $n = 12$. The samples were placed in a -20 °C
102 refrigerator prior to analysis.

2.2 EPFR analysis

104   The EPR spectrometer (MS5000, Freiberg, Germany) is used to detect EPFRs in
105 atmospheric samples. Cut the sample filter into thin strips (5 mm × 28 mm), and put it
106 into the sample tank of the quartz tissue cell (the size of the sample tank is 10 mm ×
107 30 mm)., Then the quartz tissue cell with attached filter sample was placed in a
108 resonant cavity and analyzed by an EPR spectrometer. The detection parameters were
109 magnetic field strength, 335 - 342 mT; detection time, 60 s; modulation amplitude,
110 0.20 mT; number of detections, 1; and microwave intensity, 8.0 mW. Specific testing
111 protocols have been described previously (Chen et al., 2018c).

2.3 Carbon composition analysis

113   The contents of organic carbon (OC) and elemental carbon (EC) in the filter
114 samples were analyzed using a semicontinuous OC/EC analyzer (Model 4, Sunset Lab.
115 Inc., Oregon, USA) with a NIOSH 5040 detection protocol (Lin et al., 2009).
116   The water-soluble organic carbon (WSOC) concentration was analyzed using an
117 automatic TOC-LCPH analyzer (Shimadzu, Japan). The WSOC extraction was
118 performed with ultrapure water under ultrasonication for 15 minutes, and all WSOC

119 concentrations were blank corrected. The concentration of OC in the MSM

120 (Methanol-soluble materials) was calculated as the difference between the OC and

121 WSOC (Water-soluble organic carbon) concentrations. This calculation assumes that

122 all water-insoluble organic carbon (WISOC) in the aerosol can be extracted with

123 MeOH, and the rationality of this assumption has been verified elsewhere (Mihara et

124 al., 2011; Liu et al., 2013; Cheng et al., 2016; Chen et al., 2019a).

125 *2.4 PAH analysis*

126 PAHs were detected using gas chromatography/mass spectrometry (GC/MS) on a

127 GC7890B/MS5977A (Agilent Technologies, Clara, CA). Quartz-fiber filter samples

128 (8 mm in diameter) were cut from each 25-mm quartz-fiber filter substrates used on

129 the ELPI impactor stages using a stainless-steel round punch over a clean glass dish

130 and loaded into the TD glass tube. Next, the TD glass tube was heated to 310 ℃ at a

131 rate of 12 ℃/min and thermally desorbed at 310 ℃ for 3 min. The desorbed organic

132 compounds were trapped on the head of a GC-column (DB-5MS: 5% diphenyl-95%

133 dimethyl siloxane copolymer stationary phase, 0.25-mm i.d., 30-m length, and

134 0.25-mm thickness). Sixteen target PAHs were identified based on retention time and

135 qualified ions of the standards, including 16 EPA parent PAHs (p-PAHs). The method

136 detection limits (MDLs) ranged from 0.2 pg/mm2 (Ace) to 0.6 pg/mm2 (Incdp).

137 Naphthalene-D8, acenaphthene-D10, phenanthrene-D10, chrysene-D12, and perylene

138 D12 were used for the analytical recovery check. All compounds were recovered with

139 a desorption recovery percentage of > 90%. Specific testing protocols have been

140 described previously (Han et al., 2018).

141 *2.5 Metal element analysis*

142 The concentration of metal elements in the samples was determined by a Thermo

143 X2 series inductively coupled plasma mass spectrometer (ICP-MS, Thermo, USA).

144 The metal elements analyzed in summer were Na, Mg, K, Ca, Ti, V, Cr, Mn, Fe, Co,

145 Ni, Cu, Zn, As, Cd, Pb, and Al, and those in winter were Al, Zn, V, Cr, Mn, Co, Ni, Cu,

146 As, Se, Sr, Cd, Ba, and Pb. The specific measurement method is based on the study of

147   Qi et al (2016).

2.6. Data statistics method

149   The source and formation process of EPFRs in PM with different particle sizes

150   were analyzed by nonnegative matrix factorization (NMF). The method is based on

151   the study of Chen et al (2016 and 2019e). Briefly, NMF analysis of EPFR data, metal

152   element contents, OC/EC contents and PAH contents was performed in MATLAB.

153   The version of the NMF toolbox is 1.4 (https://sites.google.com/site/nmftool/). Use

154   the gradient-based multiplication algorithm to find a solution from multiple random

155   starting values, and then use the first algorithm to find the final solution based on the

156   least squares effective set algorithm. To find a global solution, the model was run 100

157   times, each time with a different initial value. By comparing the 1-12 factor model

158   (Figure S4) with the residual of the spectral load, the 6 factor (summer) and 10 factor

159   (winter) NMF models were finally selected.

2.7. EPFR exposure evaluation

161   To assess the health risks of EPFRs, this study divided the respiratory system into

162   three parts based on the human breathing model: extrathoracic (ET) areas, including

163   the anterior nasal cavity, posterior nasal cavity, oral cavity, and throat;

164   tracheobronchial (TB) areas, including the trachea, bronchi, bronchioles, and terminal

165   bronchi; and pulmonary (P) areas, including the alveolar ducts and alveoli. Then, the

166   sedimentation rates of different particle sizes in different areas of the respiratory

167   system were determined to calculate the exposure risk of EPFRs. Here, the human

168   respiratory system particulate deposition model of Salma et al. (2002) was used, and

169   the specific data can be found in Table S3 and S4.

170   In addition, the daily inhaled concentration of EPFRs into the concentration of free

171   radicals in cigarettes were converted. The specific conversion method is as follows:

$$N_{cig} = (C_{EPFRs} \cdot V)/(RC_{cig} \cdot C_{tar}) \tag{1}$$

173   where N_{cig} represents the number of cigarettes (/person/day), C_{EPFRs} (spins/m^3)

174 represents the atmospheric concentration of EPFRs in PM, and V represents the

175 amount of air inhaled by an adult per day (20 m^3/day) (Environmental Protection

176 Agency, 1988). RC_{cig} (4.75×10^{16} spins/g) (Baum et al., 2003; Blakley et al., 2001;

177 Pryor et al., 1983; Valavanidis and Haralambous, 2001) indicates the concentration of

178 free radicals in cigarette tar, and C_{tar} (0.013 g/cig) indicates the amount of tar per

179 cigarette (Gehling et al., 2013).

3. Results and discussion

3.1 Concentrations and types of EPFRs

182 Figure 1a shows the concentration distribution of EPFRs with different particle

183 sizes in different seasons. EPFRs were detected in the particles of each tested size (the

184 EPR spectrum is shown in Figure S1), but their EPFR concentration levels were

185 different. In summer, the concentration of EPFRs in fine particles (particle size < 2.1

186 μm) is $(3.2 - 8.1) \times 10^{13}$ spins/m^3, while the concentration of EPFRs in coarse

187 particles (particle size > 2.1 μm) is 1-2 orders of magnitude higher than that of fine

188 particles, reaching values of $(2.2 - 3.5) \times 10^{14}$ spins/m^3. Winter samples show

189 completely different characteristics from summer samples. The concentration of

190 EPFRs in fine particles (particle size < 2.1 μm) is $(1.8 - 3.6) \times 10^{14}$ spins/m^3, while the

191 concentration of EPFRs in coarse particles (particle size > 2.1 μm) is smaller than that

192 of fine particles, with values of $(1.0 - 2.1) \times 10^{14}$ spins/m^3. In addition, the

193 concentration of EPFRs in particulates <0.43 μm in winter is very high, but it is very

194 low in summer. According to the results of factor analysis in part 3.2 of this study, this

195 particulate matter is related to combustion, which indicates that coal combustion in

196 winter may provide an important contribution to EPFRs. The EPFR concentration in

197 the fine PM of Linfen reported above is equivalent to that in the fine PM of Xi'an, but

198 it is ten times smaller than that in the fine PM of Beijing (Yang et al., 2017; Chen et

199 al., 2019b). Although the particle size distribution characteristics of EPFRs in winter

200 and summer are different, their concentration levels are similar, which indicates that

201 the EPFR concentration is not related to the PM concentration, but is determined by

202 the source characteristics. The source characteristics will be discussed in detail in the

203 factor analysis section.

204 Figure 1b shows the size-segregated contribution of EPFR concentration to the

205 overall. The contribution of fine PM in summer is only 14.9%, while in winter is

206 58.5%. The differences in EPFR concentrations with particle size may be related to

207 the source of EPFRs. For example, coarse particles are often associated with dust

208 sources and biogenic aerosols. In another study, the results have shown that dust

209 particles contain large amounts of metallic EPFRs and that they can be transported

210 over long distances (Chen et al., 2018b). EPFRs in fine particles may be mainly

211 derived from the combustion process, such as traffic sources, which are considered to

212 be an important source of EPFRs in atmospheric PM (Secrest et al., 2016; Chen et al.,

213 2019b). Due to winter heating in the Linfen area, the amount of coal burning increases

214 sharply in this season. In 2017, the nonclean heating (Coal-fired heating) rate of urban

215 heating energy structures in Linfen was 40% (data source: http://www.linfen.gov.cn/).

216 With the burning of coal, large amounts of EPFRs are produced, and in the summer,

217 EPFRs emitted by burning coal should be much less than those emitted in winter. This

218 can explain to a certain extent that the contribution of fine particles to summer EPFRs

219 is small, and the contribution of winter EPFRs is very large.

220 The g-factor obtained by using EPR to detect the sample is an important parameter

221 to distinguish the type of EPFR. It is the ratio of the electronic magnetic moment to its

222 angular momentum (Shaltout et al., 2015; Arangio et al., 2016). The g-factor of

223 carbon-centered persistent free radicals is generally less than 2.003, the g-factor of

224 oxygen-centered persistent radicals is generally greater than 2.004, and the g factor of

225 carbon-centered radicals with adjacent oxygen atoms is between 2.003 and 2.004

226 (Cruz et al., 2012). Figure 2a shows the g-factor distribution characteristics of EPFRs

227 in different particle sizes in summer and winter. The g-factor of fine particles and

228 coarse particles shows different characteristics. The g-factor of EPFRs in fine

229 particles (particle size < 2.1 μm) ranges from 2.0034 to 2.0037, which may be from

230 carbon-centered radicals with adjacent oxygen atoms. However, the g-factor of

231   EPFRs in coarse particles (particle size > 2.1 μm) is significantly less than that of fine

232   particles. The *g*-factor ranges from 2.0031 to 2.0033, indicating that EPFRs in coarse

233   particles are more carbon-centered than those in fine particles and are free of

234   heteroatoms. As shown in Figure 2b, the variation in the *g*-factor with concentration

235   in different season is different. The *g*-factor of summer PM showed a significant

236   decreasing trend with increasing concentration, while the *g*-factor of winter PM

237   showed a significant increasing trend with increasing EPFR concentration. Oyana et

238   al. (2017) studied EPFRs in the surface dust of leaves in the Memphis region of the

239   United States and found that the concentration of EPFRs was positively correlated

240   with the *g*-factor, and they believed that this was related to the source of EPFRs. This

241   phenomenon indicates that the sources and toxicity of EPFRs in winter and summer

242   are different.

243   *3.2 Factor Analysis of EPFRs*

244   To explore the possible sources and formation process of EPFRs in atmospheric

245   particles with different particle sizes, the NMF model was used to statistically analyze

246   EPFRs, carbon components, PAHs and metal elements in samples. The factors

247   obtained by the NMF model should reflect the different sources and generation

248   process of EPFRs. As shown in Figure 3a1 and b1, the three main contributing factors

249   to EPFRs in summer and winter are shown (see Figure S5, S6 for spectra of other

250   factors), which explain 94.5% and 83.8% of the EPFR concentrations in summer and

251   winter, respectively.

252   As shown in Figure 3a1, the typical spectral characteristic of summer factor 1 is

253   that it contains a small fraction of EC components and a large amount of OC

254   components, which indicates that combustion may be the source associated with this

255   factor. This factor has the highest loading of OC, especially WISOC; this fraction

256   mainly contains macromolecular organic substances, which are considered to

257   contribute to the main atmospheric particulate EPFRs and to be graphite oxide-like

258   substances (Chen et al., 2017; Chen et al., 2018a). Factor 2 is different from factor 1;

259   factor 2 is more likely the combustion of fossil fuels, while factor 1 should be other

combustion sources instead of burning coal, such as biomass combustion. The generation process is similar to a hybrid process, which includes the graphite oxide-like substances produced by incomplete combustion and the EPFRs formed by some metal oxides. The typical characteristic of factor 3 is that the contribution of metal elements is relatively high, while the contributions of EC and OC are very low. Metal elements such as Al, Ti, Mn, and Co are typical crust elements, so this factor may represent dust sources (Pan et al., 2013; Srivastava et al., 2007; Trapp et al., 2010). The generation process of EPFRs. The others are likely derived from the electroplating metallurgy industry (detailed in S1). As shown in Figure 3a2, the contribution ratios of different factors show that the contribution ratios of factor 1 and factor 2 are the highest, and factor 3 has only a small contribution, which indicates that combustion sources, especially incomplete combustion, are the main sources of EPFRs. The particle size distribution characteristics show that factor 1 is mainly distributed in particles larger than 2.1 μm, while factor 2 is mainly distributed in particles smaller than 0.43 μm.

The results of the factor analysis in winter are different from those in summer. As shown in Figure 3b1, the typical spectral characteristic of factor 1 is that it contains a large amount of OC components and As and Se. As and Se are trace elements of coal combustion, as shown in many studies (Pan et al., 2013; Tian et al., 2010), so coal combustion may be the source represented by this factor. From the generation process viewpoint, the factor does not contain EC, but the content of OC is very high. In the particles with a particle size of less than 3.3, which is mainly present in factor 1, the concentration of OC is 16 times that of EC. So it may be mainly a graphite oxide-like substance formed by the agglomeration of gaseous volatile organic compounds (VOCs) generated during combustion. The typical spectral characteristics of factor 2 are due to a large amount of V and some Al, EC and OC. OC and EC are also typical combustion products. V is rich in fossil fuels, especially fuel oil (Karnae et al., 2011). Therefore, traffic is the source represented by this factor. The factor contains crust elements such as Al and Mn, so it is speculated that this factor may also include

289   traffic-related dust. The typical spectral characteristics of factor 3 are similar to those

290   of factor 1, and both contain relatively large amounts of As and Se, with the exception

291   that factor 3 contains a large amount of EC, indicating that it is also mainly derived

292   from incomplete combustion sources. The generation process of factor 3 should be

293   different from factor 1, which may include both the graphite oxide-like material

294   generated by fuel coking and the EPFRs generated by the metal oxide. The other

295   factors are mainly atmospheric dust and electroplating or metallurgy (see text S1). As

296   shown in Figure 3b2, factor 1 and factor 2 have the highest proportions, and factor 3

297   also has a small contribution, which indicates that winter is the same as summer, and

298   combustion sources are the main source of EPFRs. The particle size distribution

299   characteristics show that factor 1 is mainly distributed in particles with a size of 0.43 -

300   3.3 μm, while factor 2 is mainly distributed in particles lager than 3.3 μm.

301   Based on the above analysis, it can be found that combustion sources are the main

302   sources of EPFRs, and EPFRs from these sources are mainly graphite oxide-like

303   substances generated by the polymerization of organic matter or fuel coking. Studies

304   have shown that graphene oxide can cause cell damage by generating ROS (Seabra et

305   al., 2014). The surface of these compounds contains not only carbon atoms but also

306   some heteroatoms, which leads to disorder and the presence of defects in the

307   carbon-based structure (Lyu et al., 2018; Chen et al., 2017a; Mukome et al., 2013;

308   Keiluweit et al., 2010). The dust source is also a source of important EPFRs identified

309   in this study (with a contribution of approximately 10%). It was shown in the above

310   analysis that the concentration of EPFRs in coarse particles has a significant

311   correlation with the concentration of metallic elements, particularly crustal elements.

312   Some crustal elements, such as Al, and Fe, not only have their own paramagnetism

313   (Li et al., 2017; Yu et al., 2013; Nikitenko et al., 1992), but also interact with aromatic

314   compounds attached to the surface of the particles to produce a stable single-electron

315   structure.

316   3.3 *Health risk of EPFRs*

317   To evaluate the health risks of EPFRs in PM with different particle sizes, this study

318   evaluated the comprehensive exposure of EPFRs based on the deposition efficiency of

319   PM with different particle sizes in different parts of the human body. The results are

320   shown in Figure 4a. The ET region is the region with the highest EPFR exposure,

321   while the TB and P regions have relatively close EPFRs. This result shows that

322   atmospheric EPFRs are the most harmful to the health of the human upper respiratory

323   tract. Comparing the EPFR exposure in different seasons indicates that the exposure

324   risk in the ET area in summer is significantly higher than that in winter. This

325   difference occurs because the concentration of EPFRs in coarse particles is much

326   higher than that of fine particles in summer and the deposition efficiency of large

327   particles in the ET area is generally higher. Fine particles are more efficiently

328   deposited in the P region, leading to a higher risk of EPFR exposure in the P region in

329   winter.

330   EPFRs were found early in cigarette tar and are considered one of the health risk

331   factors in cigarette smoke (Lyons et al., 1960); thus, in this study, the exposure risks

332   of EPFRs in particles deposited in the human body were converted to the equivalent

333   number of cigarettes inhaled per adult per day. As shown in Figure 4b, the ET area is

334   the most contaminated area, with an average equivalence of twenty-one cigarettes

335   (twenty-five in summer and sixteen in winter). The average values for the TB area

336   (nine in summer and seven in winter) and P area (seven in summer and ten in winter)

337   are eight. The results indicate that EPFRs pose significant health risks to human lungs

338   in both winter and summer. Other similar studies, such as a study of the average

339   amount of EPFRs in $PM_{2.5}$ inhaled per person per day in Xi'an in 2017, found values

340   equivalent to approximately 5 cigarettes (Chen et al., 2018a). Gehring and Dellinger

341   (2013) found that EPFR exposure in $PM_{2.5}$ is equivalent to approximately 0.3

342   cigarettes per person per day in St. Joaquin County, the location with the worst air

343   pollution in the United States. The average exposure risk of EPFRs in fine particles in

344   the Linfen area (approximately 13 cigarettes) was higher than those in these two

345   studies. However, these previous studies only studied the exposure risk of EPFRs in

346   fine particles. The results of this study indicate that the health risks of EPFRs are

significantly increased when the particle size distribution of EPFRs is taken into account. Therefore, it is important to study the source characteristics and generation process of EPFRs with different particle sizes, which will be discussed in detail in the following sections.

This study calculated the proportion of EPFRs with different particle sizes in different parts of the respiratory system based on the deposition efficiency of particles with different particle sizes. As shown in Figure 4c, in the ET region and the TB region, coarse particles are the dominant component in summer and winter. In particular, in summer, the proportion of EPFRs in coarse particles in these two regions exceeds 95%. In the P region, there are significant differences between summer and winter. The P region in summer is still dominated by coarse particles, but its proportion is significantly lower than those in the ET and TB regions. In the P region in winter, fine particles are the dominant component (approximately 70%). These distribution characteristics indicate different sources of EPFRs in different regions. As shown in Figure 4d, in summer, combustion sources are the main source of EPFRs in the respiratory system. In winter, combustion and transportation sources contribute equally in the EP and ET regions, while in the alveoli, combustion sources are the main contributor. The ET region is the area with the highest risk of exposure to EPFRs (21 cigarettes). The generation process of these EPFRs is mainly attributable to graphene oxide-like substances. Studies have shown that graphene oxide is cytotoxic (Harmon et al., 2018). In the alveoli, the contribution of combustion sources is significantly increased (especially in winter). These EPFRs are mainly generated by the action of metal oxides and organic substances. Studies have shown that such EPFRs can generate ROS in the lung fluid environment (Khachatryan et al., 2011).

4. **Conclusions and environmental implications**

This study systematically reported the particle size distribution of EPFRs in atmospheric PM in Linfen, which is one of the most polluted cities in China and is located in a typical coal-burning area. In addition, this study evaluated the

comprehensive health risks of EPFRs, and reported possible sources and formation process of atmospheric EPFRs with respect to different particle sizes. The following main conclusions were obtained.

(1) This study found that EPFRs are widely present in atmospheric particles of different particle sizes and exhibit significant particle size distribution characteristics. The results of this study demonstrate that the concentrations and types of EPFRs are dependent on particle size and season. This seasonal characteristic of EPFRs is mainly affected by the PM sources, this result also indicates that the potential toxicity caused by EPFRs may also vary with particle size and season.

(2) This study reported the possible source and formation process of atmospheric EPFRs in different particle sizes. The results show that combustion is the most important source of EPFRs (>70%) in both winter and summer PM samples in Linfen. The graphite oxide-like process has the highest contribution (~70%) and is mainly distributed in particles with a size of > 0.43 μm. These findings deepen our understanding of the pollution characteristics of atmospheric EPFRs and are useful for controlling EPFR generation in heavily polluted areas.

(3) This study assessed the exposure risk of EPFRs in different areas of the respiratory system. The results show that the upper respiratory tract is the area with the highest EPFR exposure. The trachea and alveoli are also exposed to EPFRs, and the risk of exposure is equivalent to that of 8 cigarettes per person per day. Coarse particles are the main source of EPFRs in the upper respiratory tract, while fine particles are mainly involved in the alveoli.

Through this study, the results have shown that there are significant differences in the concentrations and types of EPFRs in particles of different sizes and these differences are due to the influence of the source and generation process. In the future, assessments of the particle size distribution and the seasonality of EPFRs in atmospheric PM should be considered. Health risks are another focus of this study. It is found that the upper respiratory tract is the key exposure area of EPFRs, and the traffic source is the main source of EPFRs in this area. This finding is significant for a

systematic assessment of the health risks of EPFRs. In view of the complexity and diversity of the formation process of EPFRs in actual atmospheric particulates, the relative contributions of EPFRs generated by different process and their associated health risks should be more comprehensively studied in the future.

Acknowledgments

Appendix A. Supplementary data

Appendix A contains additional details, including the EPR spectra of samples of different particle sizes, correlations between EPFRs and carbon in particles of different particle sizes, the results and errors of factor analysis, correlation analysis of EPFRs with metallic elements, and EPFR exposure in different areas of the human respiratory tract.

Code/Data availability: All data that support the findings of this study are available in this article and its Supplement or from the corresponding author on request.

Author contribution: Qingcai Chen: Research design, Methodology, Writing - Original Draft, Writing - Review & Editing, Project administration, Funding acquisition; Haoyao Sun: Investigation, Sample analysis, Writing - Original Draft, Writing - Review & Editing, Methodology, Formal analysis; Wenhuai Song: Investigation, Sample collection, Chemical analysis; Fang Cao: Investigation, Sample collection; Chongguo Tian: Investigation, Chemical analysis; Yan-Lin Zhang: Conceptualization, Writing - Review & Editing, Formal analysis, Validation, Funding acquisition.

Competing interests: The authors declare that they have no conflict of interest.

References

Arangio, A. M., Tong, H., Socorro, J., Pöschl, U., Shiraiwa, M., 2016. Quantification of environmentally persistent free radicals and reactive oxygen species in atmospheric aerosol particles. Atmos. Chem. Phys. 16 (20), 13105–13119.

Blakley, R. L., Henry, D. D., Smith, C. J., 2001. Lack of correlation between cigarette mainstream smoke particulate phase radicals and hydroquinone yield. Food. Chem. Toxicol. 39 (4), 401−406.

Baum, S.L., Anderson, I.G.M., Baker, R.R., Murphy, D.M., Rowlands, C.C., 2003. Electron spin resonance and spin trap investigation of free radicals in cigarette smoke: development of a quantification procedure. Anal. Chim. Acta 481, 1−13.

Cruz, A.L.N.D., Cook, R.L., Lomnicki, S.M., Dellinger, B., 2012. Effect of low temperature thermal treatment on soils contaminated with pentachlorophenol and environmentally persistent free radicals. Environ. Sci. Technol. 46, 5971−5978.

Chen, N., Huang, Y., Hou, X., Ai, Z., Zhang, L., 2017. Photochemistry of hydrochar: Reactive oxygen species generation and sulfadimidine degradation. Environ. Sci. Technol. 51 (19), 11278−11287.

Chen, Q., Mu. Z., Song, W., Wang, Y., Yang, Z., Zhang, L., Zhang, Y., 2019a. Size-resolved characterization of the chromophores in atmospheric particulate matter in Linfen, China. J. Geophys. Res-Atmos. 124, DIO: 10.1029/2019JD031149.

Chen, Q., Ikemori, F., Nakamura Y., Vodicka, P., Kawamura, K., Mochida, M., 2017. Structural and light-absorption characteristics of complex water-insoluble organic mixtures in urban submicron aerosols. Environ. Sci. Technol. 51(15), 8293−8303.

Chen, Q., Miyazaki, Y., Kawamura, K., Matsumoto, K., Coburn, S., Volkamer, R., Iwamoto, Y., Kagami, S., Deng, Y., Ogawa, S., 2016. Characterization of chromophoric water-soluble organic matter in urban, forest, and marine aerosols by HR-ToF-AMS analysis and excitation–emission matrix spectroscopy. Environ. Sci. Technol. 50 (19), 10351–10360.

Chen, Q., Sun, H., Mu, Z., Wang, Y., Li, Y., Zhang, L., Wang, M., Zhang, Z., 2019b. Characteristics of environmentally persistent free radicals in PM2.5: Concentrations, species and sources in Xi'an, Northwestern China. Environ. Pollut. 247, 18−26.

Chen, Q., Sun, H., Wang, J., Shan, M., Xue, J., Yang, X., Deng, M., Wang, Y., Zhang, L., 2019c. Long-life type — The dominant fraction of EPFRs in combustion sources and ambient fine particles in Xi'an. Atmos. Environ. 219, 117059.

Chen, Q., Sun, H., Wang, M., Mu, Z., Wang, Y., Li, Y., Wang, Y., Zhang, L., Zhang, Z., 2018a. Dominant fraction of EPFRs from Nonsolvent-Extractable organic matter in fine particulates over Xi'an, China. Environ. Sci. Technol. 52 (17), 9646−9655.

Chen, Q., Sun, H., Wang, M., Wang, Y., Zhang, L., Han, Y., 2019d. Environmentally persistent free radical (EPFR) formation by visible-light illumination of the organic matter in atmospheric particles. Environ. Sci. Technol, 53 (17), 10053−10061.

Chen, Q., Wang, M., Sun, H., Wang, X., Wang, Y., Li, Y., Zhang, L., Mu, Z., 2018b. Enhanced health risks from exposure to environmentally persistent free radicals and the oxidative stress of PM2.5 from asian dust storms in erenhot, Zhangbei and Jinan, China. Environ. Int. 123, 260−268.

Chen, Q., Wang, M., Wang, Y., Zhang, L., Li, Y., Han, Y., 2019e. Oxidative potential of water-soluble matter associated with chromophoric substances in PM2.5 over Xi'an, China. Environ. Sci. Technol, 53 (17), 10053−10061.

Chen, Q., Wang, M., Wang, Y., Zhang, L., Xue, J., Sun, H., Mu, Z., 2018c. Rapid determination of environmentally persistent free radicals (EPFRs) in atmospheric particles with a quartz sheet-based approach using electron paramagnetic resonance (EPR) spectroscopy. Atmos. Environ. 184, 140−145.

Cheng, Y., He, K. B., Du, Z. Y., Engling, G., Liu, J. M., Ma, Y. L., Zheng, M., Weber, R. J., 2016. The characteristics of brown carbon aerosol during winter in Beijing. Atmos. Environ. 127, 355–364.

Cormier, S. A., Lomnicki, S., Backes, W., Delliger, B., 2006. Origin and health impacts of emissions of toxic by-products and fine particles from combustion and thermal treatment of hazardous wastes and materials. Environ. Health. Perspect. 114 (6), 810−817.

D'Arienzo, M., Gamba, L., Morazzoni, F., Cosention, U., Creco, C., Lasagni, M., Pitea, D., Moro, G., Cepek, C., Butera, V., Sicilia, E., Russo, N., Muñoz-García, A., Pavone, M., 2017. Experimental and theoretical investigation on the catalytic generation of environmentally persistent free radicals from benzene. J. Phys. Chem. A. 121 (17), 9381−9393.

Dellinger, B., Lomnicki, S., Khachatryan, L., Maskos, Z., Hall, R. W., Adounkpe, J., McFerrin, C., Truong, H., 2007. Formation and stabilization of persistent free radicals. Proc. Combust. Inst. 31 (1), 521−528.

Dellinger, B., Pryor, W. A., Cueto, R., Squadrito, G. L., Hegde, V., Deutsch, W. A., 2001. Role of free radicals in the toxicity of airborne fine particulate matter. Chem. Res. Toxicol. 14 (10), 1371−1377.

Environmental Protection Agency, 1988. Recommendations for and Documentation of Biological Values for Use in Risk Assessment. PB-179874. EPA 600/6-87/008. US Environmental Protection Agency, Cincinnati, OH.

Finkelstein, E., Rosen, G. M., Rauckman, E. J., 1982. Production of hydroxyl radical by decomposition of superoxide spin-trapped adducts. Mol. Pharmacol. 21 (2), 262–265.

Gehling, W., Dellinger, B., 2013. Environmentally persistent free radicals and their lifetimes in PM2.5. Environ. Sci. Technol. 47 (15), 8172−8178.

Han, Y., Chen, Y. J., Saud, A., Feng, Y. L., Zhang, F., Song, W. H., Cao, F., Zhang, Y., Yang, X., Li, J., Zhang, G., 2018. High time- and size-resolved measurements of PM and chemical composition from coal combustion: Implications for the EC formation process. Environ. Sci. Technol. 52 (11), 6676–6685.

Harmon, A. C., Hebert, V. Y., Cormier, S. A., Subramanian, B., Reed, J. R., Backes, W. L., Dugas, T. R., 2018. Particulate matter containing environmentally persistent free radicals induces AhRdependent cytokine and reactive oxygen species production in human bronchial epithelial cells. Plos. One. 13 (10), e0205412.

Karnae, S., John, K., 2011. Source apportionment of fine particulate matter measured in an industrialized coastal urban area of South Texas. Atmos. Environ. 45 (23), 3769−3776.

Keiluweit, M., Nico, P. S., Johnson, M. G., Kleber, M., 2010. Dynamic molecular structure of plant biomass-derived black carbon (biochar). Environ. Sci. Technol. 44 (4), 1247−1253.

Khachatryan, L., Dellinger, B., 2011. Environmentally persistent free radicals (EPFRs)-2. Are free hydroxyl radicals generated in aqueous solutions?. Environ. Sci. Technol. 45 (21), 9232−9239.

Li, G. L., Wu, S. Y., Kuang, M. Q., Hu, X. F., Xu, Y. Q., 2017. Studies on the g-factors of the copper(II)-oxygen compounds. J. Struct. Chem. 58 (4), 700−705.

Lin, P., Hu, M., Deng, Z., Slanina, J., Han, S., Kondo, Y., Takegawa, N., Miyazaki, Y., Zhao, Y., Sugimoto, N., 2009. Seasonal and diurnal variations of organic carbon in PM2.5 in Beijing and the estimation of secondary organic carbon. J. Geophys. Res-Atmos. 114, 1−41.

Liu, J., Bergin, M., Guo, H., King, L., Kotra, N., Edgerton, E., Weber, R. J., 2013. Size-resolved measurements of brown carbon in water and methanol extracts and estimates of their contribution to ambient fine-particle light absorption. Atmos. Chem. Phys. 13, 12389–12404.

Lomnicki, S., Truong, H., Vejerano, E., Delliger, B., 2008. Copper oxide-based model of persistent free radical formation on combustion-derived particulate matter. Environ. Sci. Technol. 42 (13), 4982−4988.

Lyu, L., Yu, G., Zhang, L., Hu, C., Sun, Y., 2018. 4-Phenoxyphenolfunctionalized reduced graphene oxide nanosheets: A metal-free fenton-like catalyst for pollutant destruction. Environ. Sci. Technol. 52 (2), 747−756.

Lyons, M.J., Spence, J.B., 1960. Environmental free radicals. Br. J. Canc. 14, 703−708

Mihara, T., Michihiro, M., 2011. Characterization of solvent-extractable organics in urban aerosols based on mass spectrum analysis and hygroscopic growth measurement. Environ. Sci. Technol. 45 (21), 9168–9174.

Mukome, F. N. D., Zhang, X., Silva, L. C. R., Six, J., Parikh, S. J., 2013. Use of Chemical and physical characteristics to investigate trends in biochar feedstocks. J. Agric. Food Chem. 61 (9), 2196−2204.

Nikitenko, V. A., 1992. Luminescence and EPR of zinc oxide (review). J. Appl. Spectrosc. 57 (5–6), 783–798.

Oyana, T. J., Lomnicki, S. M., Guo, C., Cormier, S. A., 2017. A scalable field study protocol and rationale for passive ambient air sampling: a spatial phytosampling for leaf data collection. Environ. Sci. Technol. 51 (18), 10663−10673.

Pan, Y., Wang, Y., Sun, Y., Tian, S., Cheng, M., 2013. Size-resolved aerosol trace elements at a rural mountainous site in Northern China: importance of regional transport. Sci. total Environ. 461−462, 761−771.

Patterson, M. C., Keilbart, N. D., Kiruri, L. W., Thibodeaux, C. A., Lomnicki, S., Kurtz, R. L., Poliakoff, E. D., Dellinger, B., Sprunger, P. T., 2013. EPFR formation from phenol adsorption on Al2O3 and TiO2: EPR and EELS studies. Chem. Phys. 422, 277−282.

Pryor, W.A., Prier, D.G., Church, D.F., 1983. Electron-spin resonance study of mainstream and sidestream cigarette smoke: nature of the free radicals in gas-phase smoke and in cigarette tar. Environ. Health Perspect. 47, 345−355.

Pryor, W. A., 1986. Oxy-Radicals and Related Species: Their Formation, Lifetimes, and Reactions. Annu. Rev. Physiol. 48, 657–667.

Qi, L., Zhang, Y., Ma, Y., Chen, M., Ge, X., Ma, Y., Zheng, J., Wang, Z., Li, S., 2016. Source identification of trace elements in the atmosphere during the second Asian Youth Games in Nanjing, China: Influence of control measures on air quality. Atmos. Pollut. Res. 7, 547–556.

Shaltout, A. A., Boman, J., Shehadeh, Z. F., Al-Malawi, D. A. R., Hemeda, O. M., Morsy, M. M., 2015. Spectroscopic investigation of PM2.5, collected at industrial, residential and traffic sites in taif. Saudi Arabia. J. Aerosol. Sci. 79, 97−108.

Srivastava, A., Jain, V. K., 2007. Size distribution and source identification of total suspended particulate matter and associated heavy metals in the urban atmosphere of Delhi. Chemosphere. 68(3), 579−589.

Strak, M., Janssen, N. A. H., Godri, K. J., Gosens, I., Mudway, I. S., Cassee, F. R., Lebret, E., Kelly F. J., Harrison, R. M., Brunekreef, B., Steenhof, M., Hoek, G., 2012. Respiratory health effects of airborne particulate matter: The role of particle size, composition, and oxidative potential—the RAPTES project. Eviron. Health. Persp. 120 (8), 1183–1189.

Salma, I., Balásházy, I., Winkler-Heil, R., Hofmann, W., Záray, G. 2002. Effect of particle mass size distribution on the deposition of aerosols in the human respiratory tract. J. Aerosol. Sci. 33(1), 119-132.

Seabra A.B., Paula A.J., Lima R. D., Alves. O.L., Durán. N. 2014. Nanotoxicity of graphene and graphene oxide. Chem. Res. Toxicol. 27 (2), 159–168.

Thevenot, P. T., Saravia, J., Jin, N., Giaimo, J. D., Chustz, R. E., Mahne, S., Kelley, M. A., Hebert, V. Y., Dellinger, B., Dugas, T. R., Demayo, F. G., Cormier, S. A., 2013. Radical-containing ultrafine particulate matter initiates epithelial-to-mesenchymal transitions in airway epithelial cells. Am. J. Respir. Cell. Mol. Biol. 48 (2), 188−197.

Tian, H., Wang, Y., Xue, Z., Cheng, K., Qu, Y., Chai, F., Hao, J., 2010. Trend and characteristics of atmospheric emissions of Hg, As, and Se from coal combustion in China, 1980−2007. Atmos. Chem. Phys. 10 (23), 11905−11919.

Tong, H., Lakey, P. S. J., Arangio, A. M., Socorro, J., Shen, F., Lucas, K., Brune, W. H., Pöschl, U., Shiraiwa, M., 2018. Reactive oxygen species formed by secondary organic aerosols in water and surrogate lung fluid. Environ. Sci. Technol. 52 (20), 11642−11651.

Trapp, J. M., Millero, F. J., Prospero, J. M., 2010. Temporal variability of the elemental composition of African dust measured in trade wind aerosols at Barbados and Miami. Mar. Chem. 120 (1-4), 71−82.

Truong, H., Lomnicki, S., Dellinger, B., 2010. Potential for misidentification of environmentally persistent free radicals as molecular pollutants in particulate matter. Environ. Sci. Technol. 44 (6), 1933−1939.

Valavanidis, A., Fiotakis, K., Vlachogianni, T., 2008. Airborne particulate matterand human health: toxicological assessment and importance of size and composition of particles for oxidative damage and carcinogenic mechanisms. J. Environ. Sci. Heal. C. 26 (4), 339–362.

Vejerano, E. P., Rao, G., Khachatryan, L., Cormier, S. A., Lomnicki, S., 2018. Environmentally persistent free radicals: Insights on a new class of pollutants. Environ. Sci. Technol. 52 (5), 2468−2481.

Vejerano, E., Lomnicki, S. M., Dellinger, B., 2012a. Formation and stabilization of combustion-generated, environmentally persistent radicals on Ni(II)O supported on a silica surface. Environ. Sci. Technol. 46 (17), 9406−9411.

Vejerano, E., Lomnicki, S., Dellinger, B., 2011. Formation and stabilization of combustion-generated environmentally persistent free radicals on an Fe(III)2O3/silica surface. Environ. Sci. Technol. 45 (2), 589−594.

Valavanidis, A., Haralambous, E., 2001. A comparative study by electron paramagnetic resonance of free radical species in the mainstream and sidestream smoke of cigarettes with conventional acetate filters and 'bio-filters. Redox. Rep. 6, 161−171.

Vejerano, E., Lomnicki, S., Dellinger, B., 2010. Formation and stabilization of combustion-generated environmentally persistent free radicals on an Fe(III) 2O3/silica surface. Environ. Sci. Technol. 45 (2), 589−594.

Vejerano, E., Lomnicki, S., Dellinger, B., 2012b. Lifetime of combustion-generated environmentally persistent free radicals on Zn(II)O and other transition metal oxides. J. Environ. Monit. 14 (10), 2803−2806.

Wang, P., Pan, B., Li, H., Huang, Y., Dong, X., Fang, A., Liu, L., Wu, Min., Xing, B., 2018. The overlooked occurrence of environmentally persistent free radicals in an area with low-rank coal burning, Xuanwei, China. Environ. Sci. Technol. 52 (3), 1054−1061.

Wang, Y., Li, S., Wang, M., Sun, H., Mu, Z., Zhang, L., Li, Y., Chen, Q., 2019. Source apportionment of environmentally persistent free radicals (EPFRs) in PM2.5 over Xi'an, China. Sci. Total. Environ. 689, 193–202.

Yang, L., Liu, G., Zheng, M., Jin, R., Zhu, Q, Zhao, Y., Wu, X., Yang, X., 2017. Highly elevated levels and particle-size distributions of environmentally persistent free radicals in haze-associated atmosphere. Environ. Sci. Technol. 51 (14), 7936−7944.

Yu, T., Wang, J., Shen, M., Li, W., 2013. NH3-SCR over Cu/SAPO-34 catalysts with various acid contents and low Cu loading. Catal. Sci. Technol. 3 (12), 3234–3241.
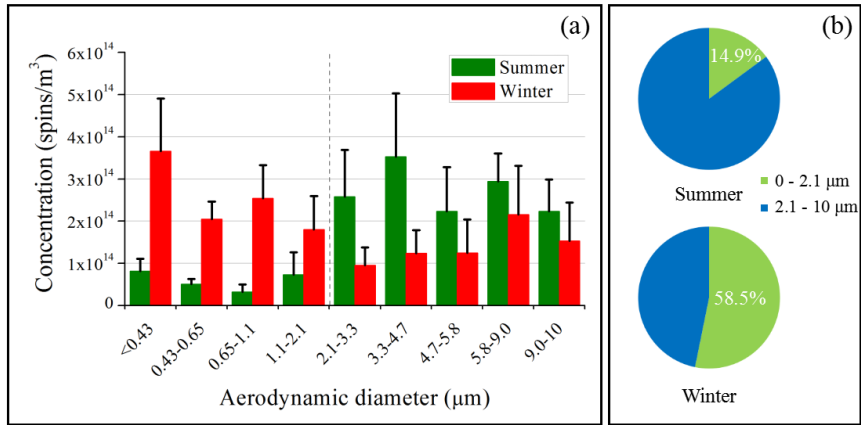
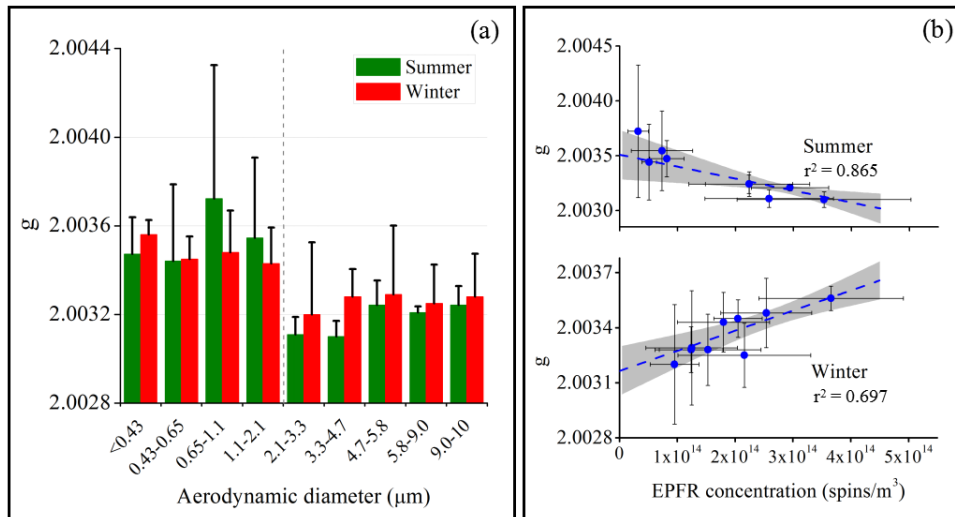Figure 1. The concentration of EPFRs in PM with different particle sizes. (a) Atmospheric concentrations of EPFRs in different particle sizes in summer and winter. (b) The relative contribution of fine particles and coarse particles to the total EPFR concentration.

626

Figure 2. A *g*-factor comparison. (a) Comparison of *g*-factors of EPFRs in different particle sizes in different seasons. (b) Correlation analysis of *g*-factors and concentrations of EPFRs in summer and winter PM. The gray areas in the figure represent 95% confidence intervals.

630
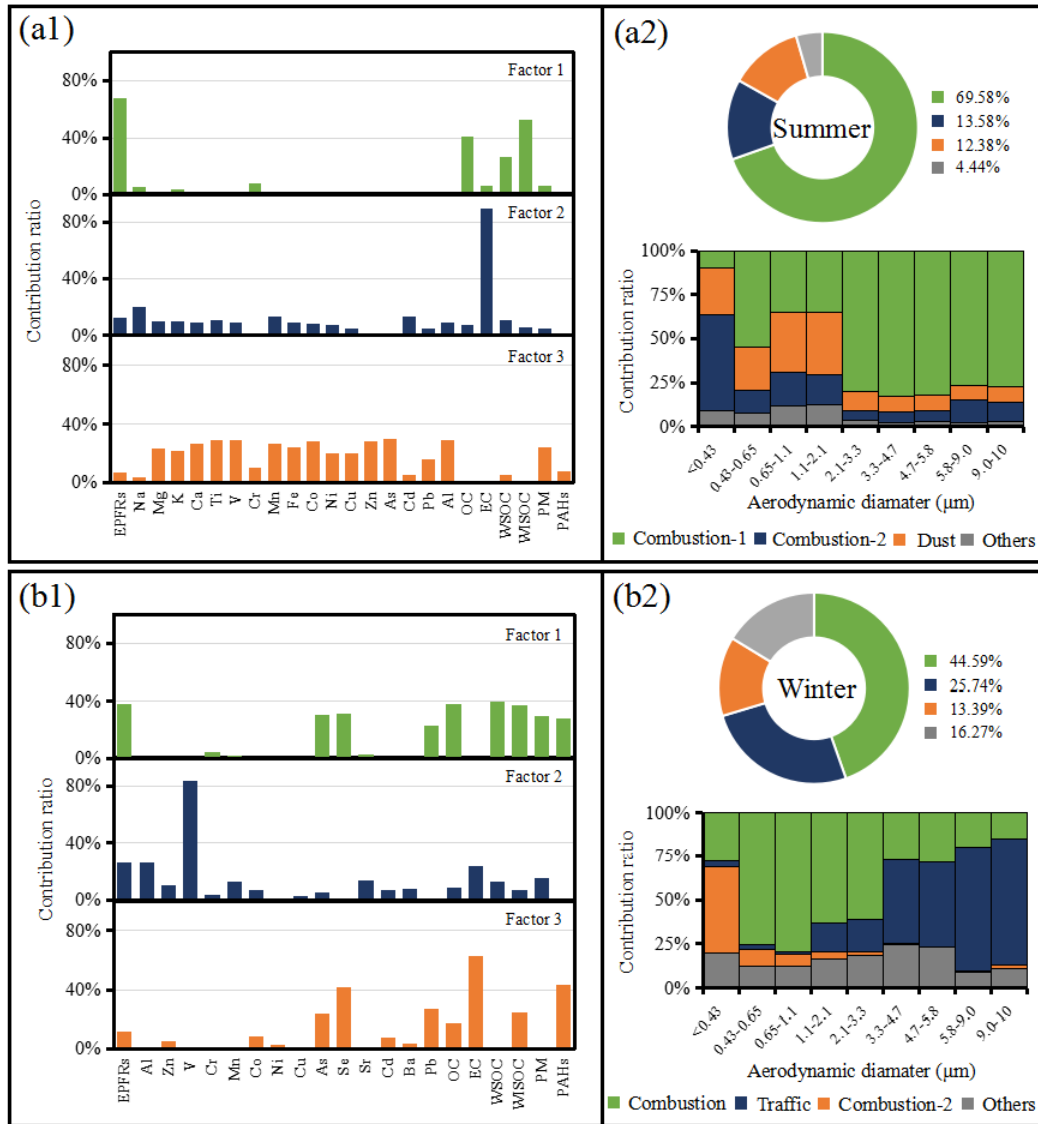
Figure 3. Factor analysis of EPFRs in different particle sizes in different seasons. (a1) and (b1)

represent the results of factor analysis for summer and winter, respectively. (a2) and (b2) represent

the contribution of various factors in summer and winter, respectively, to EPFRs and the relative

contributions of each factor for different particle sizes.
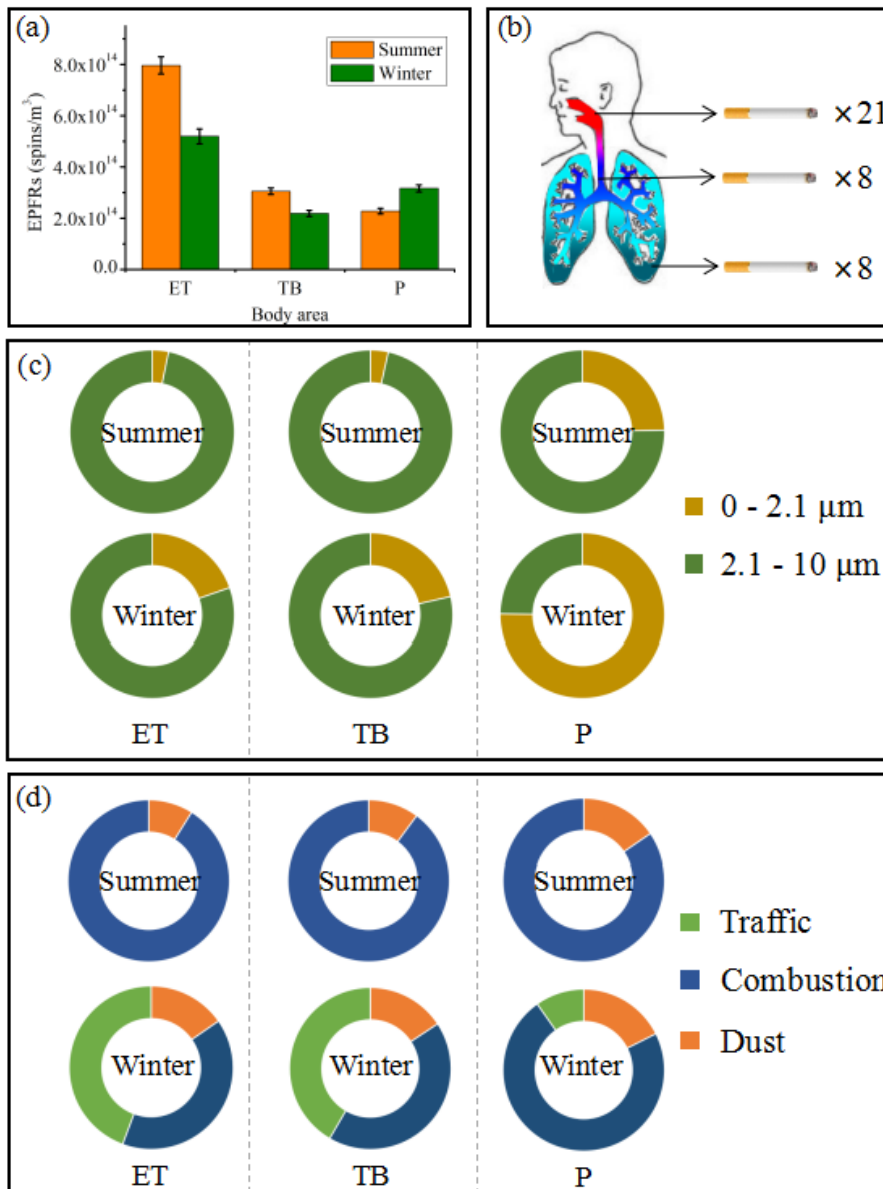
Figure 4. Exposure risks to EPFRs. (a) EPFR exposure in the ET, TB, and P regions. (b) Cigarette exposure to EPFRs in the human respiratory system. (c) Exposure ratio of EPFRs with different particle sizes in different areas of the respiratory system. (d) Contribution of EPFRs from different sources to different areas of the respiratory system.